Supporting Information: Anion distribution, structural distortion, and symmetry-driven optical band gap bowing in mixed halide Cs_2SnX_6 vacancy ordered double perovskites

Maham M. S. Karim,[1] Alex M. Ganose,[1,2,3] Laura Pieters,[1] W. W. Winnie Leung,[1] Jessica Wade,[4] Lina Zhang,[1] David O. Scanlon,[1,2,3] Robert G. Palgrave*[1]

1. Department of Chemistry, University College London, 20 Gordon Street, London, WC1H 0AJ, United Kingdom

2. Diamond Light Source Ltd., Diamond House, Harwell Science and Innovation Campus, Didcot, Oxfordshire OX11 0DE, United Kingdom

3. Thomas Young Centre, University College London, Gower Street, London WC1E 6BT, United Kingdom

4. Department of Physics and Centre for Plastic Electronics, Imperial College London, SW7 2AZ, United Kingdom

* Corresponding Author: Email: r.palgrave@ucl.ac.uk

Nominal composition (n)	Mean experimental composition (n)	**Lattice parameter, *a* / Å**	**Halide (x, 0, 0)**	**M-X bond length / Å**
0	**0**	10.3573(1)	0.2331(3)	2.4146(4)
0.17	**0.01**	10.3573(1)	0.2332(3)	2.4154(4)
0.25	**0.065**	10.3856(1)	0.2346(3)	2.4366(4)
0.33	**0.12**	10.4100(1)	0.2348(3)	2.4442(4)
0.5	**0.17**	10.4555(1)	0.2361(3)	2.4694(4)
0.67	**0.21**	10.4569(1)	0.2366(3)	2.4741(4)
0.75	**0.51**	10.5969(1)	0.2389(3)	2.5316(7)
0.83	**0.78**	10.7041(2)	0.2393(4)	2.5616(6)
0.92	**0.83**	10.7484(2)	0.2388(4)	2.5678(6)
0.95	**0.84**	10.7540(2)	0.2395(3)	2.5763(5)
0.98	**0.94**	10.7857(4)	0.2403(3)	2.5919(7)
1	**1**	10.8035(4)	0.2388(4)	2.5806(8)

Table S1. Composition and structural information on the $Cs_2Sn(Br_nCl_{1-n})_6$ series of compounds.

Estimated standard deviations in the last reported significant figure appear in brackets

Nominal Composition (n)	Mean experimental composition (n)	**Lattice parameter, *a* / Å**	**Halide (x, 0, 0)**	**M-X bond length / Å**
0	**0**	10.8035(1)	0.2388(4)	2.5806(5)
0.17	**0.020**	10.8456(1)	0.2390(3)	2.5928(4)
0.25	**0.048**	10.8666(1)	0.2406(3)	2.6150(4)
0.33	**0.077**	10.9081(1)	0.2401(3)	2.6198(4)
0.5	**0.18**	11.0315(2)	0.2403(3)	2.6511(5)
0.67	**0.44**	11.1710(2)	0.2413(3)	2.6964(5)
0.75	**0.52**	11.3160(1)	0.2425(2)	2.7446(3)
0.83	**0.69**	11.3943(3)	0.2431(3)	2.7704(6)
0.92	**0.88**	11.5387(1)	0.2443(2)	2.8200(3)
0.95	**0.92**	11.5690(1)	0.2443(2)	2.8269(3)
0.98	**0.97**	11.6032(1)	0.2441(2)	2.8331(3)
1	**1.00**	11.6152(2)	0.2447(1)	2.8430(3)

Table S2. Composition and structural information on the $Cs_2Sn(I_nBr_{1-n})_6$ series of compounds. Estimated standard deviations in the last reported significant figure appear in brackets

Geometrical consideration of A_2BX_6 structure

From figure S1 it can be seen that

$$d(X_\alpha X_\alpha) = \sqrt{2}(r_B + r_X) = \sqrt{2}ax \quad \text{(S1)}$$

where *a* is the lattice parameter and *x* is the crystallographic coordinate of the halide ion. It can also be shown that the ratio between $d(X_\alpha X_\beta)$ and $d(X_\alpha X_\alpha)$ is given by:

$$\frac{d(X_\alpha X_\beta)}{d(X_\alpha X_\alpha)} = \frac{1}{2x} - 1$$

And thus for $x = 0.25$, $d(X_\alpha X_\beta) = d(X_\alpha X_\alpha)$. A hypothetical A_2BX_6 vacancy ordered perovskite structure with x = 0.25 has the same halide sublattice as is found in the *Pm-3m* cubic perovskite structure. Recall equation 3 from the main manuscript, which defines R as the ratio of the size of the A site cation to the cavity in which it sits:

$$R = \frac{r_A + r_X}{\frac{1}{2}[d(X_\alpha X_\beta) + d(X_\alpha X_\alpha)]}$$

In the case that $x = 0.25$, $d(X_\alpha X_\beta) = d(X_\alpha X_\alpha)$ and therefore:

$$R = \frac{r_A + r_X}{d(X_\alpha X_\alpha)}$$

And through substitution of equation S1, we derive the Goldschmidt Tolerance factor:

$$R = \frac{r_A + r_X}{\sqrt{2}(r_B + r_X)}$$

which is therefore a special case of equation 3 when x = 0.25, which is true in the case of a cubic ABX_3 perovskite.

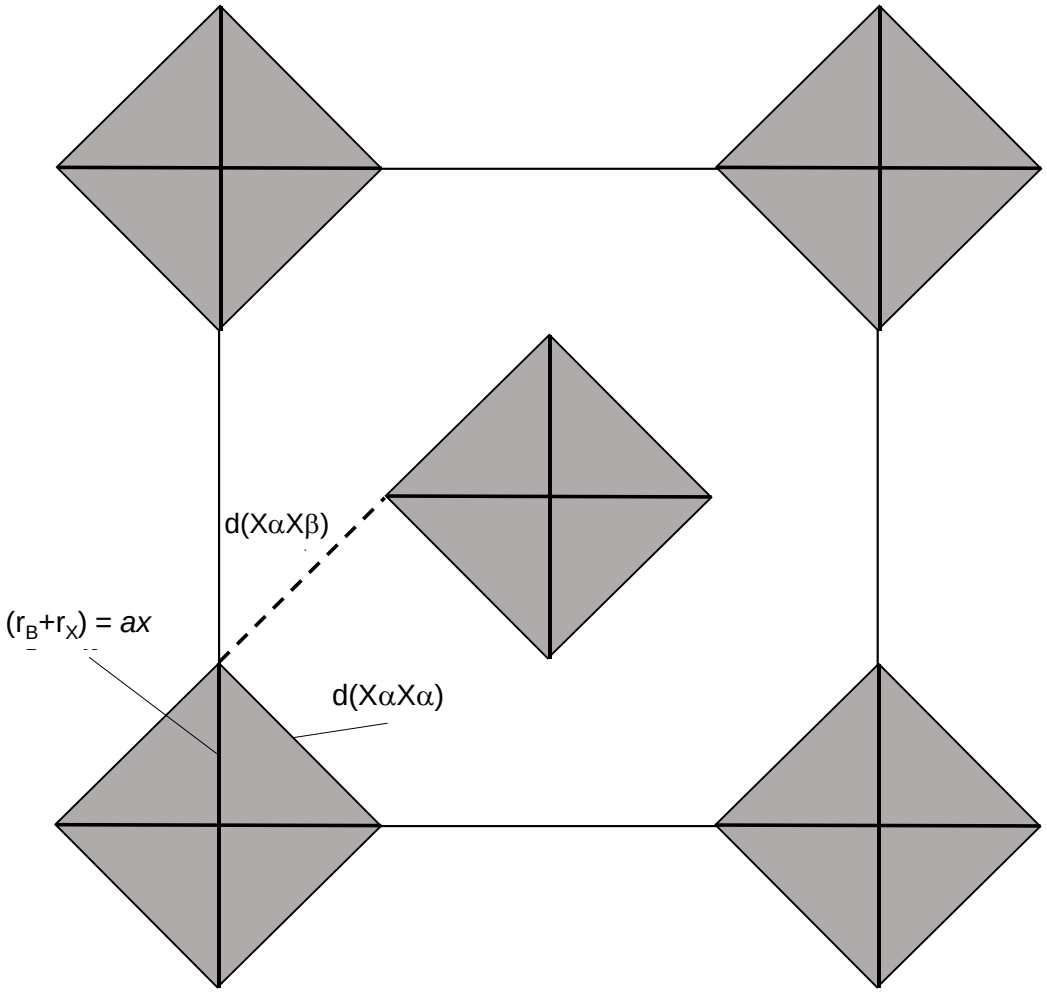

Figure S1. A face of the cubic A_2BX_6 unit cell. Shaded squares represent sections of BX_6 octahedra, with the vertices marking the centres of the halide (X) ions. Three relevant distances are indicated: $d(X_\alpha X_\alpha)$, the shortest interhalogen distance within an octahedron, $d(X_\alpha X_\beta)$, the shortest interhalogen distance between two octahedra, and the B-X bond length, which, assuming the hard sphere model, equals the sum of the ionic radii of B and X (r_B and r_X respectively) and is also equal to the product of the lattice parameter, *a*, and the crystallographic coordinate of the halide ion, *x*.

Distribution of halide ions and octahedral types

We consider the distribution of halide ions in mixed halide Cs_2SnX_6 compounds. If the halide ions are randomly placed throughout the structure, the resulting distribution of octahedral types can be determined. The analysis below is presented for the chloride-bromide series, but the same argument applies to the bromide-iodide series.

For an individual octahedron, in the mixed chloride bromide series there are seven possible overall compositions: $SnBr_xCl_{(6-x)}$ with *x* taking integers from 0-6. The number of combinations of *x* bromide ions from 6 halide ions coordinated to the Sn is:

$$C(6,x) = \frac{6!}{(6-x)!\,x!}$$

Given random halide distribution, the probability of a particular X site ion being occupied by a bromide ion, p(Br), is given by:

$$\mathrm{p(Br)} = \frac{[\mathrm{Br}]}{[\mathrm{Br}] + [\mathrm{Cl}]}$$

where [Br] and [Cl] are the overall bromine and chlorine concentrations respectively. We measure this quantity experimentally as described in the main manuscript.

Thus the probability of an octahedron $[SnBr_xCl_{(6-x)}]^{2-}$ forming with a given p(Br) is:

$$\mathrm{p(x)} = C(6,x) \times \mathrm{p(Br)}^{x} \times (1 - \mathrm{p(Br)})^{(6-x)}$$

For x = 2,3,4 there are two distinct isomers for each x value: *cis/trans* and *fac/mer* isomers. Again assuming random placement of X site ions, *fac* and *mer* isomers are equally likely while *cis* isomers are four times as likely as *trans* isomers.

An example of the distribution of octahedra types for a hypothetical p(Br) = 0.5, i.e. the compound $A_2SnCl_3Br_3$ is shown in Figure S2.

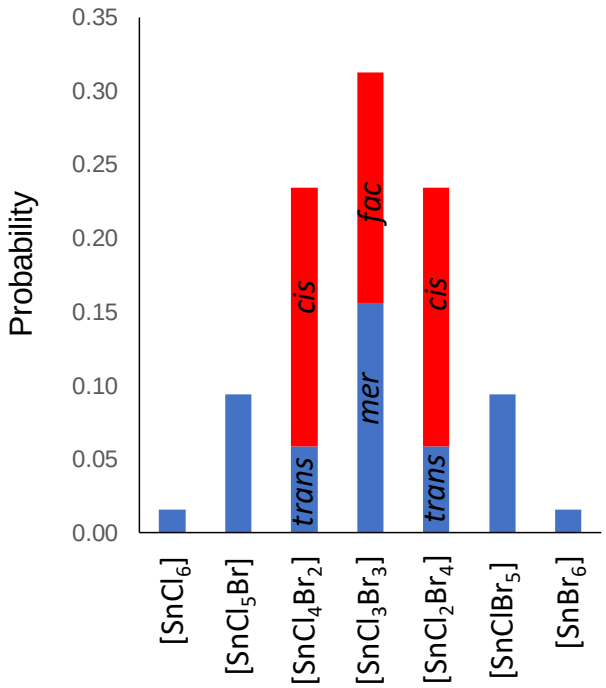

Figure S2. Probability distribution of octahedra types in $A_2SnCl_3Br_3$, assuming random distribution of halide ions throughout the structure.

Calculation of Raman spectra for mixed halide compounds

The Raman spectrum of each octahedral type was calculated as described in the main manuscript (to summarise, a 50:50 Gaussian:Lorentzian peak with FWHM between 3-5 cm^{-1}). The results for each octahedral type are shown in Figure S3 below.

These spectra can be summed in different proportions to give simulated spectra for compounds containing different proportions of each octahedra. In this way, the simulated spectra in Figure S3 were summed according to the calculated distribution of octahedral types, such as that shown in Figure S2, to yield a simulated Raman spectrum for a given composition. We emphasise that this simulated spectra assumes random distribution of the halide ions with no regard for the thermodynamic stability of the resultant $[SnX_6]^{2-}$ octahedra. We calculate Raman spectra for such randomly distributed halide ions for different $Cs_2Sn(I_nBr_{1-n})_6$ and $Cs_2Sn(Br_nCl_{1-n})_6$ compositions and these are shown in Figure S4, below. Note that the addition of a small amount of iodine to Cs_2SnBr_6 results in large changes to the simulated Raman spectrum, so several spectra are shown in S4 with

very low levels of iodide, which compare to several of our samples described in the main manuscript.

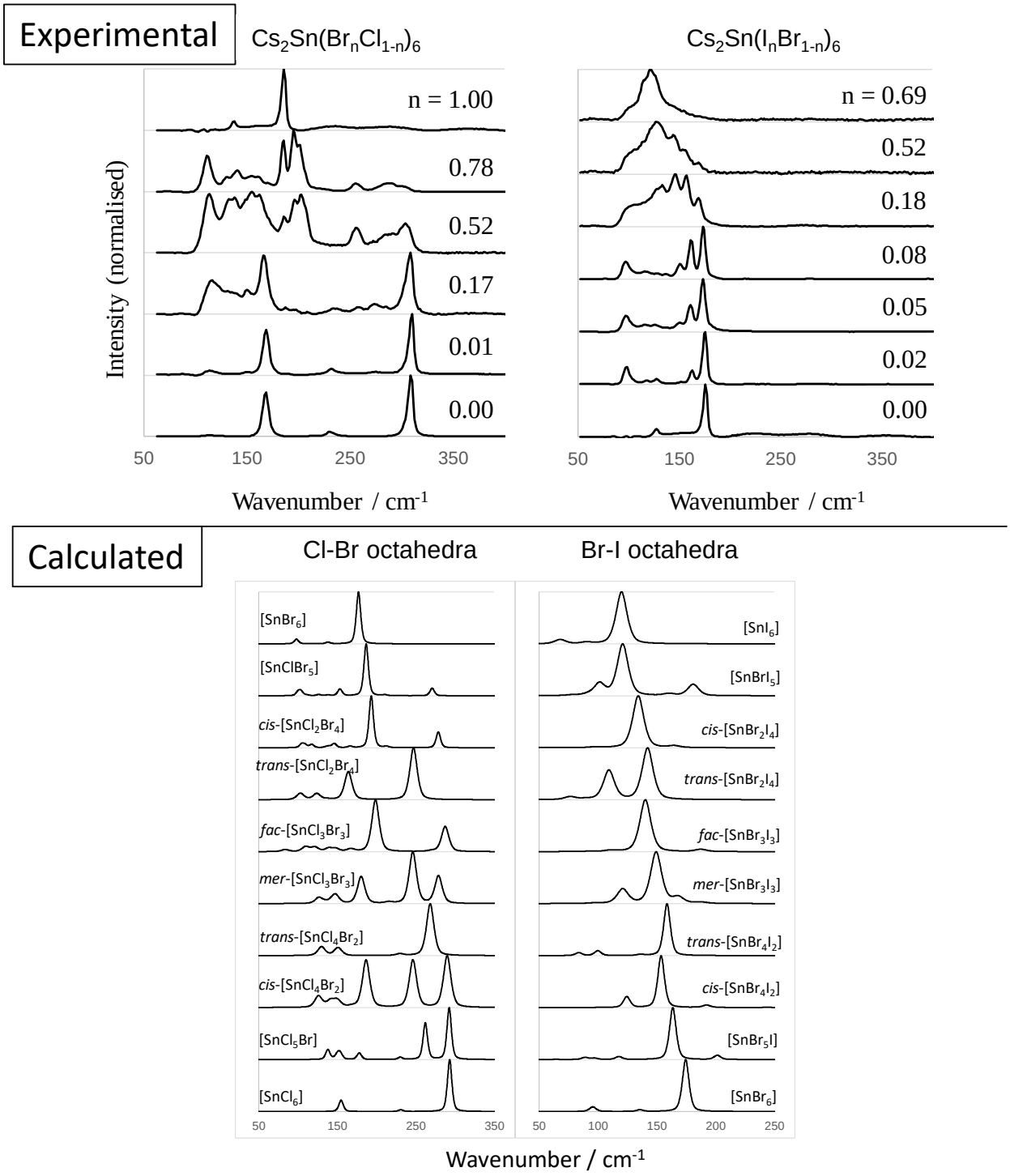

Figure S3. Top: Experimental Raman spectra from Cs_2SnX_6 samples with mixed halides. Bottom: Calculated Raman spectra for $[SnX_6]^{2-}$ octahedra consisting of mixed chloride-bromide or bromide-iodide ligands. Raman spectra were calculated using DFPT with the PBEsol functional.

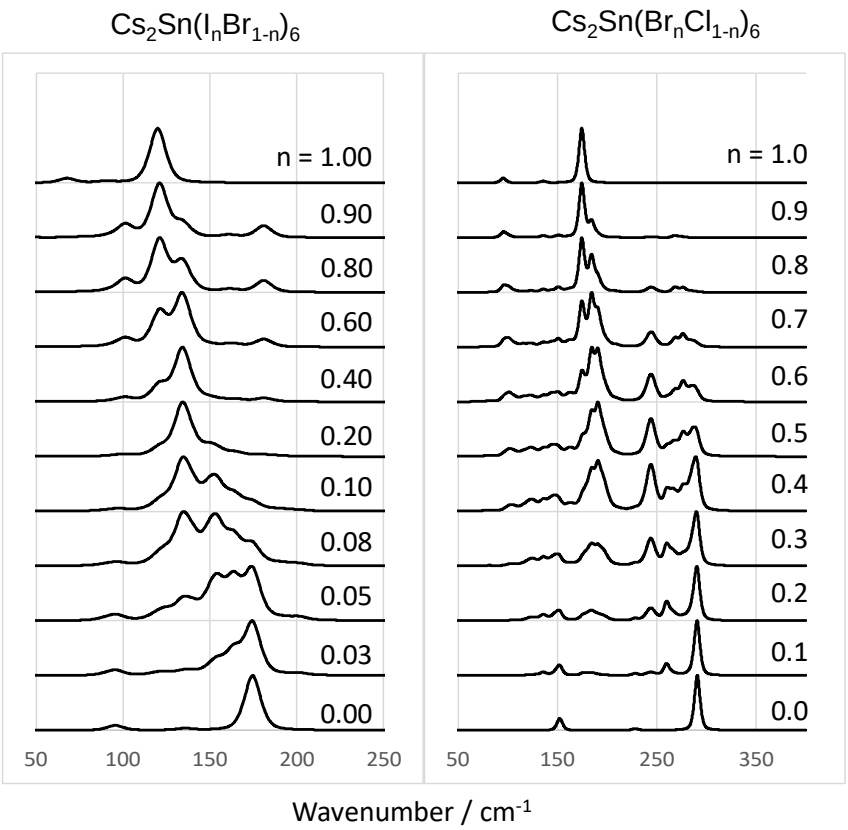

Figure S4. Calculated Raman spectra for mixed halide Cs_2SnX_6 samples with random distribution of halide ions. For each composition, *n*, the concentration of each $[SnX_6]^{2-}$ octahedron type is calculated and the Raman spectra summed in proportion to their concentration.

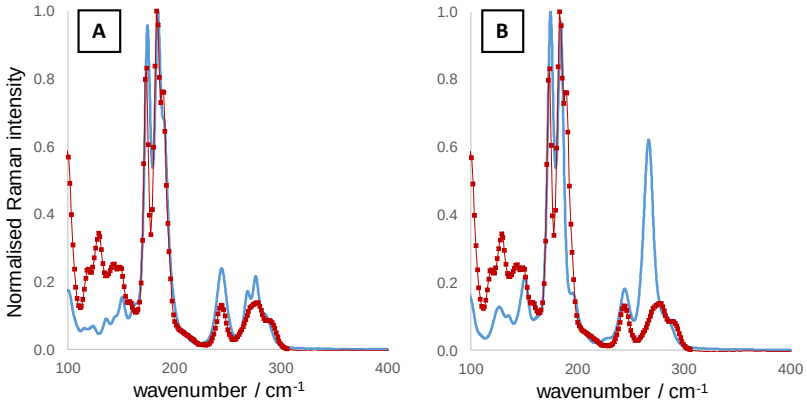

Figure S5. Calculated (blue lines) and experimental (red points) Raman spectra for $Cs_2SnCl_{1.32}Br_{4.68}$. A) Calculated Raman spectrum uses a random distribution of halides B) Calculated Raman spectrum uses an identical model to A except that all SnX_2Y_4 octahedra present are in the cis configuration. Even this small change causes a significant difference in the calculated spectrum, such that the model fits much less well to the experimental data compared with the random distribution model.

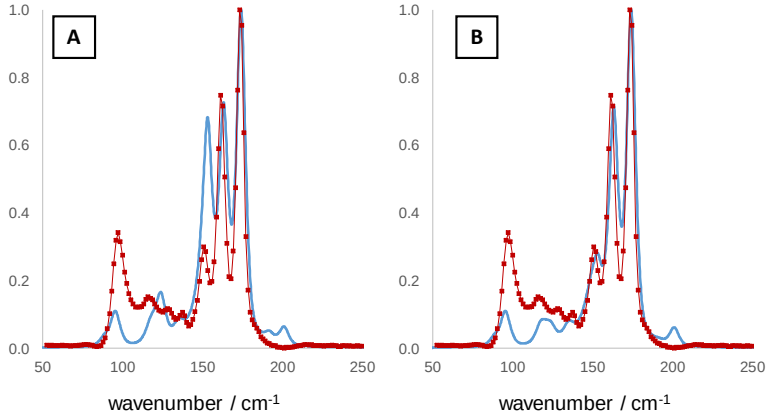

Figure S6. Calculated (blue lines) and experimental (red points) Raman spectra for $Cs_2SnBr_{5.54}I_{0.46}$. A) Calculated Raman spectrum uses a random distribution of halides B) Calculated Raman spectrum uses an identical model to A except that the concentration of cis-$[SnBr_4I_2]$ octahedra has been reduced by a factor of 4, and these octahedra converted to trans-$[SnBr_4I_2]$ octahedra. This change causes the model to reproduce the experimental spectral shape in the 150-180 cm^{-1} region very well.

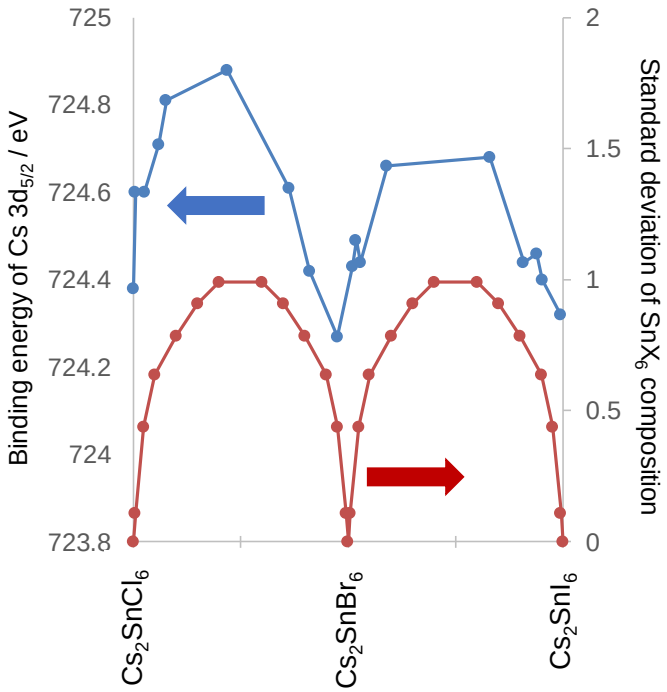

Figure S7. Correlation between Cs $3d_{5/2}$ binding energy from XPS and the standard deviation of the SnX_6 composition distribution, for different compositions of Cs_2SnX_6. The Cs $3d_{5/2}$ binding energy seems to correlate with the multiplicity of octahedra present.

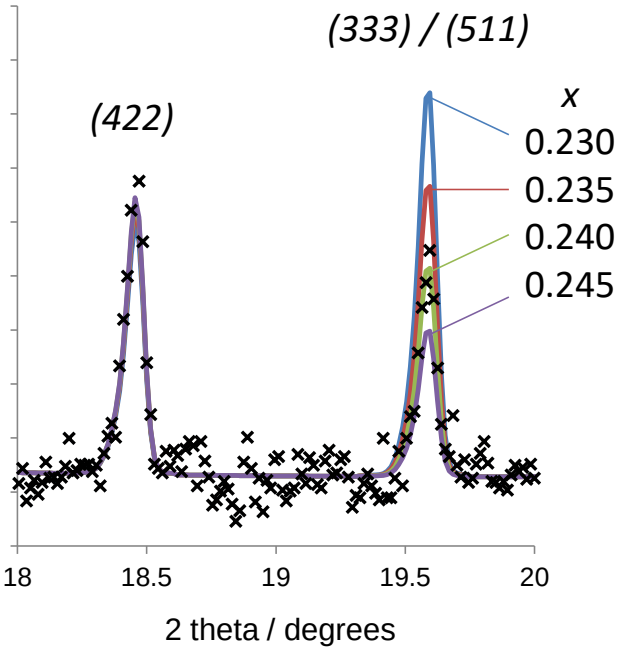

Figure S8. Diffraction pattern recorded from Cs_2SnCl_6 (black crosses), along with four modelled diffraction patterns (solid lines) which vary only in the crystallographic parameter, *x*, which denotes the position of the halide anion (at crystallographic coordinates *(x,0,0)*) and thus defines the M-X bond length. Changes in *x* cause significant intensity variation in (*hhh*) peaks, as can be seen this is detectable by the lab XRD measurements used here. Other (*hhh*) diffraction peaks are similarly affected.

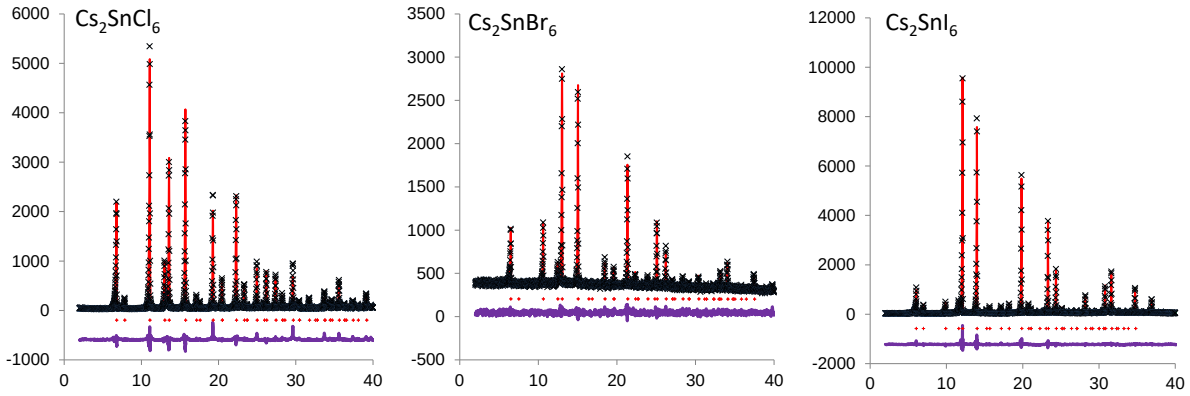

Figure S9. Rietveld refinements on the pure halide compounds Cs_2SnCl_6, Cs_2SnBr_6 and Cs_2SnI_6. Black crosses represent experimental powder XRD data, red lines represent the PXRD pattern calculated from the final refined model. Red tick marks show the expected reflection positions based on the model ,and the purple line shows the difference between experimental and calculated patterns.

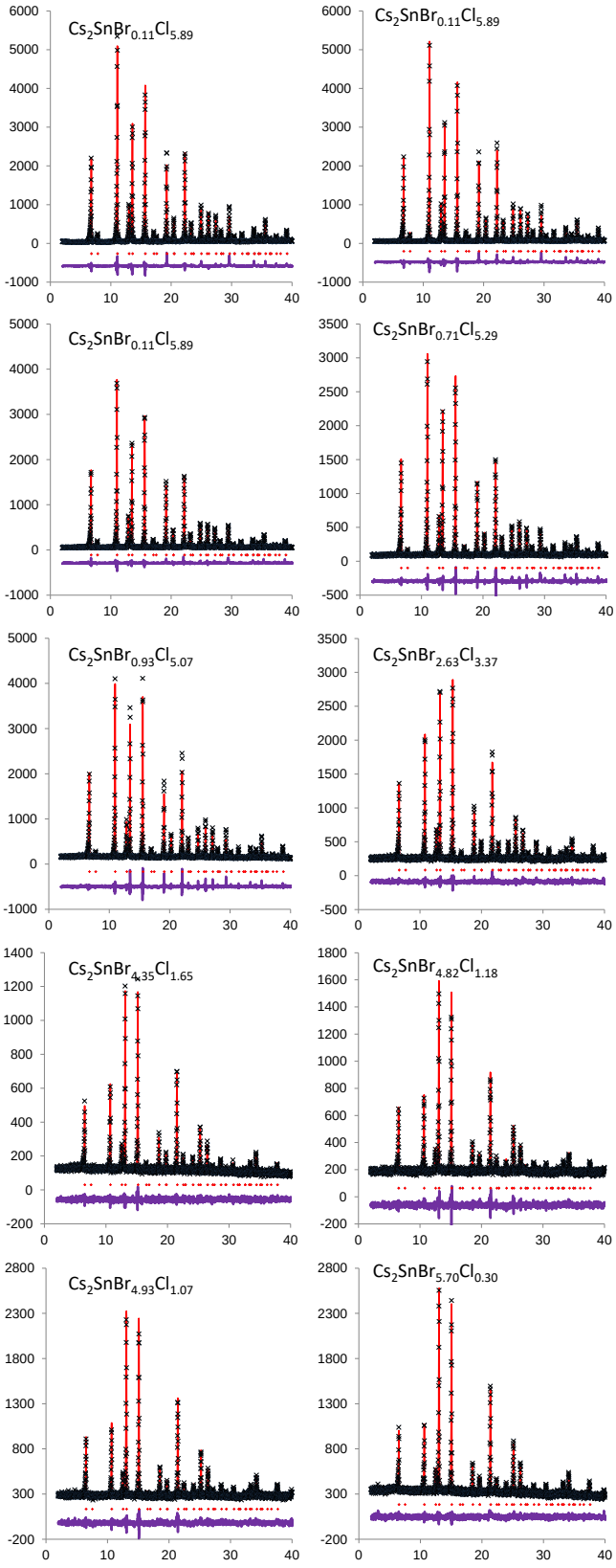

Figure S10. Rietveld refinements of mixed halide compounds $Cs_2Sn(Br_nCl_{1-n})_6$. Black crosses represent experimental powder XRD data, red lines represent the PXRD pattern calculated from the final refined model. Red tick marks show the expected reflection positions based on the model, and the purple line shows the difference between experimental and calculated patterns.

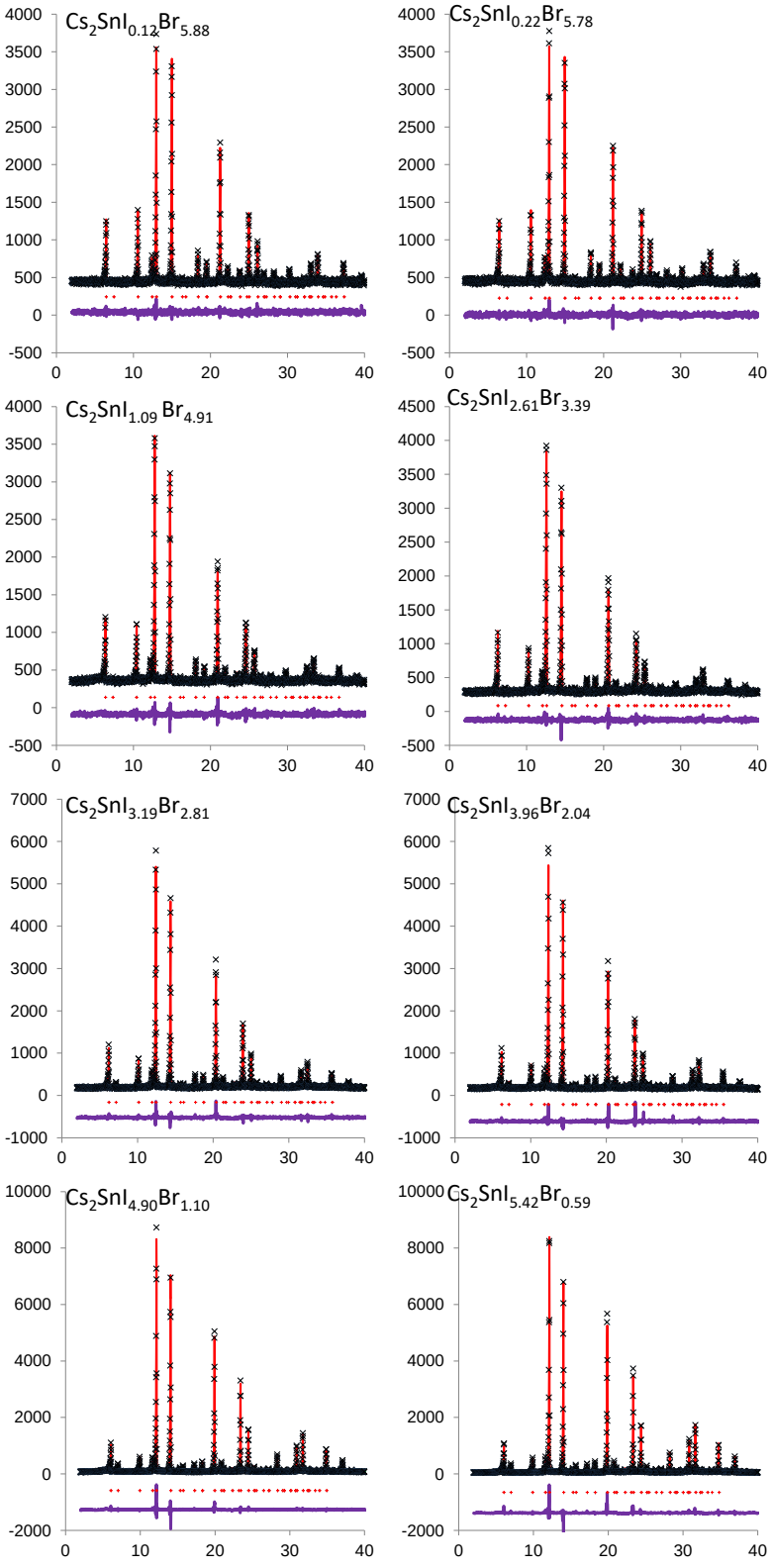

Figure S10. Rietveld refinements of mixed halide compounds $Cs_2Sn(I_nBr_{1-n})_6$. Black crosses represent experimental powder XRD data, red lines represent the PXRD pattern calculated from the final refined model. Red tick marks show the expected reflection positions based on the model, and the purple line shows the difference between experimental and calculated patterns.

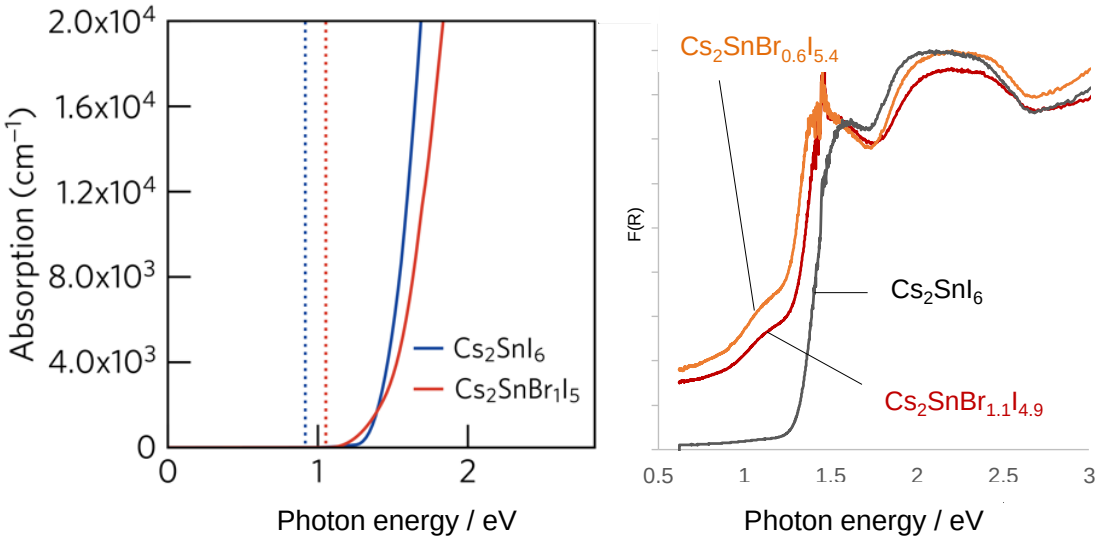

Figure S11. Optical properties of Cs_2SnX_6 compounds. Left: Optical absorption spectra of Cs_2SnI_6 and $Cs_2SnBr_1I_5$ calculated using HSE06+SOC, shown by solid blue and red lines, respectively. The fundamental band gaps for each compound are shown by dashed lines and highlight the difference between the optical and fundamental band gaps. Right: Normalised optical spectra of Cs_2SnI_6 and two iodine rich, mixed bromide-iodide compounds, both of which show absorption features below the Cs_2SnI_6 band edge

Larger A site cations

Mixed halide A_2SnX_6 compounds where A = $CH_3NH_3^+$ and $CH_3CH_2NH_3^+$ (A = MA^+ and EA^+) were studied. MA_2SnX_6 and EA_2SnX_6 compounds were synthesised in the same way as the A = Cs series, except that an aqueous solution of methylamine or ethylamine was reacted with the appropriate hydrohalic acid or mixture of acids to produce an acidic solution of alkylammonium halide. This was mixed with the ethanolic solutions of SnX_4 corresponding to the desired halide composition. In contrast to the synthesis of Cs containing products, the MA and EA series

crystallised much more slowly, forming a solid product over a period of minutes for chloride rich samples to several days for the iodide rich samples.

For the series with A = MA^+, in the chloride-bromide series, none of the compounds formed in the cubic *Fm-3m* structure. XRD patterns were indexed in the *R-3m* space group following analysis by Kitahama *et al*. and for each halide composition a single phase was present. The structure can be thought of as layers of isolated BX_6 octahedra in the *ab* plane with A cations in the interlayer spacing. The lattice volume increased with increasing halide mass, as shown in Figure S12, although the *c* parameter remained almost constant with increasing halide mass, whilst an increase was observed in the *a* parameter, indicating that the lattice expansion occurs mainly through expansion of the B-X layers rather than increasing the interlayer spacing. A similar pattern is seen in the EA_2SnX_6 series from chloride to bromide, which adopts the same *R-3m* structure and undergoes lattice expansion with increasing bromide content through expansion of *a* whilst *c* remains almost constant. The $MA_2Sn(I_nBr_{1-n})_6$ compounds could not be reliably synthesised by the solution phase method which was successful for the other compounds discussed here. Instead we used a high temperature route whereby methylammonium halide was combined with the tin tetrahalide in the appropriate quantities and heated in a quartz tube at 200 ^oC. All compounds formed in the $MA_2Sn(I_nBr_{1-n})_6$ series were found to adopt the cubic *Fm-3m* structure as seen in their Cs analogues. We could not form single phase compounds in the interval $0 < n < 0.17$, and we expect in this region the *R-3m* and *Fm-3m* structures are very similar in energy.

Figure S12 shows the unit cell volume per formula unit of A_2SnX_6 compounds. As can be seen in the A = MA^+ series there appears to be no discontinuity in lattice volume associated with the compositionally driven cubic-rhombohedral phase transition.

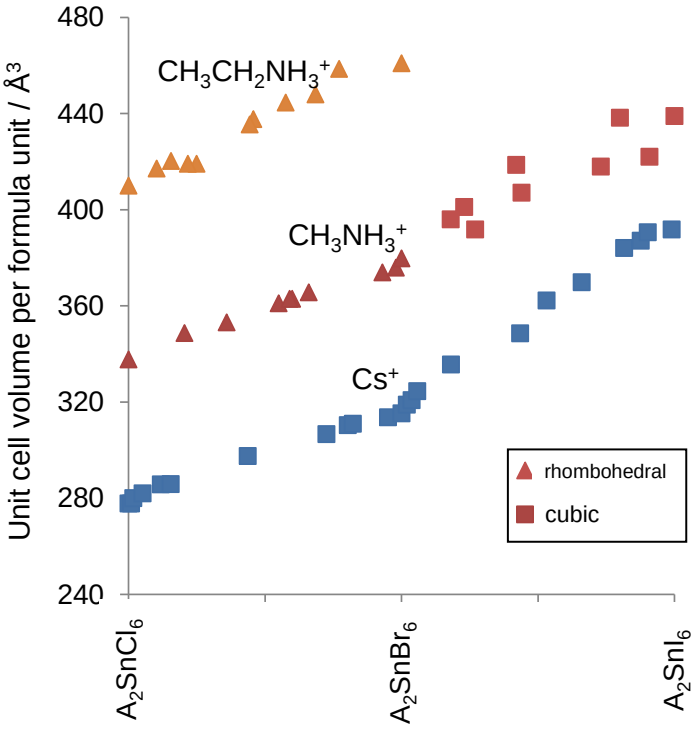

Figure S12. Lattice volumes of A_2SnX_6 compounds with A = Cs^+, MA^+, EA^+ and X = Cl, Br, I and mixtures thereof. The shape of the data point represents the crystal structure of the compound as indicated in the figure key.

Nominal composition (n)	XPS composition (n)	XRF composition (n)	XRD composition (n)
0	0	0	0
0.17	0.01	0.01	0.00
0.25	0.04	0.10	0.00
0.33	0.10	0.16	0.025
0.5	0.12	0.22	0.12
0.67	0.16	0.26	0.15
0.75	0.48	0.54	0.48
0.83	0.73	0.82	0.77
0.92	0.79	0.87	0.87
0.95	0.81	0.88	0.89
0.98	0.91	0.97	0.99
1	1	1	1

Table S3. Composition measurements on the $Cs_2Sn(Br_nCl_{1-n})_6$ series of compounds. NB in the manuscript the 'experimental composition' is an average of the XPS and XRF measurements.

Nominal composition (n)	XPS composition (n)	XRF composition (n)	XRD composition (n)
0	0	0	0
0.17	0.030	0.01	0
0.25	0.048	0.02	0
0.33	0.087	0.04	0
0.5	0.18	0.07	0.18
0.67	0.44	0.35	0.35
0.75	0.53	0.45	0.47
0.83	0.69	0.64	0.59
0.92	0.88	0.87	0.74
0.95	0.92	0.93	0.83
0.98	0.97	0.98	0.85
1	1	1	1

Table S4. Composition measurements on the $Cs_2Sn(I_nBr_{1-n})_6$ series of compounds. NB in the manuscript the 'experimental composition' is an average of the XPS and XRF measurements.

Compound	Calculated fundamental band gap / eV	Calculated optical band gap / eV	Measured optical band gap / eV
Cs_2SnCl_6	4.17	4.50	4.89
Cs_2SnBr_6	2.54	2.85	3.23
Cs_2SnI_6	0.92	1.26	1.35
$Cs_2SnCl_5Br_1$	3.82	3.82	N/A
$Cs_2SnCl_1Br_5$	2.71	2.71	N/A
$Cs_2SnBr_1I_5$	1.05	1.05	N/A
$Cs_2SnBr_5I_1$	1.93	1.93	N/A

Table S5. Calculated fundamental and optical band gaps for Cs_2SnX_6 compounds. Note that for mixed halide compounds, the calculation use a model with only one type of tin halide octahedron. Real samples with the same composition will contain a distribution of tin halide octahedra as discussed in the main manuscript.